

Possible three dimensional nodes in the  $s_{\pm}$  superconducting gap of  $\text{BaFe}_2(\text{As}_{1-x}\text{P}_x)_2$ Katsuhiro Suzuki<sup>1,2</sup>, Hidetomo Usui<sup>1</sup>, and Kazuhiko Kuroki<sup>1,2</sup><sup>1</sup> Department of Applied Physics and Chemistry, The University of Electro-Communications, Chofu, Tokyo 182-8585, Japan<sup>2</sup> JST, TRIP, Chofu, Tokyo 182-8585, Japan

We examine theoretically the superconducting state of  $\text{BaFe}_2(\text{As}_{1-x}\text{P}_x)_2$ , an isovalent doping 122 iron pnictide superconductor. We construct a three dimensional ten orbital model from first principles band calculation, and investigate the superconducting gap within the spin fluctuation mediated pairing mechanism. The gap is basically  $s_{\pm}$ , where the gap changes its sign between electron and hole Fermi surfaces, but three dimensional nodal structures appear in the largely warped hole Fermi surface having strong  $Z^2/XZ/YZ$  orbital character. The present result, together with our previous study on 1111 systems, explains the strong material dependence of the superconducting gap in the iron pnictides.

KEYWORDS: 122 iron pnictides, superconducting gap, spin fluctuations, first principles band calculation

It is now becoming more and more clear that the superconducting gap of the iron pnictides<sup>1</sup> has nonuniversal forms. A number of experiments have suggested presence of fully open gap,<sup>2,3</sup> but for  $\text{LaFePO}$  in particular, experiments suggest presence of line nodes in the gap.<sup>4-6</sup> In a previous study, motivated by an experimental observation by Lee *et al.*,<sup>7</sup> we have mainly focused on the 1111 systems, and pointed out that the band structure around the wave vector  $(\pi, \pi)$  in the unfolded Brillouin zone, and thus superconductivity, is sensitive to the pnictogen height measured from the iron plane.<sup>8</sup> Using a five orbital model,<sup>9</sup> we have shown that when the pnictogen is at high positions, the  $X^2 - Y^2$  band around  $(\pi, \pi)$  gives a hole Fermi surface, and in this case, the spin fluctuations arising from the interaction between electron and hole Fermi surfaces give rise to a fully gapped  $s_{\pm}$ -wave pairing.<sup>9-12</sup> On the other hand, as the pnictogen is lowered, the  $Z^2$  band around  $(\pi, \pi)$  rises up above the Fermi level while the  $X^2 - Y^2$  band sinks below. This results in the presence of line nodes in the superconducting gap either in the nodal  $s_{\pm}$ -wave form, where the gap nodes are on the electron Fermi surfaces, or in the  $d$ -wave form where the nodes are on the hole Fermi surfaces.<sup>9,13</sup> Fluctuation exchange (FLEX)<sup>14</sup> and functional renormalization group<sup>15,16</sup> studies also find similar tendency. The presence of line nodes in the superconducting gap results in a lower  $T_c$ , and this explains the experimental observation of lines nodes in the low  $T_c$   $\text{LaFePO}$ .<sup>4-6</sup>

However, if we turn to the 122 materials, there are now several experiments that do not fit into this view. In the isovalent doping system  $\text{BaFe}_2(\text{As}_{1-x}\text{P}_x)_2$ ,<sup>17,18</sup> a number of experiments suggest presence of line nodes in the superconducting gap,<sup>19,20</sup> but  $T_c$  is relatively high (maximum  $T_c$  of about 30K),<sup>18</sup> in contrast to  $\text{LaFePO}$ . Moreover, the  $X^2 - Y^2$  hole Fermi surface is found to be present in this material theoretically (as seen below), and this seems to be supported also in an angle resolved photoemission (ARPES) experiment.<sup>21</sup> Another interesting observation in the 122 materials is the possible presence of nodes in the superconducting gap of  $\text{KFe}_2\text{As}_2$ .<sup>22-26</sup> In this material, the electron Fermi surface is barely

present,<sup>27</sup> so it is strongly likely that the gap nodes are on the hole Fermi surface. Here also, the  $X^2 - Y^2$  hole Fermi surface should be present because there is a large amount of holes. These experimental observations for the 122 materials do not seem to fit into the view that nodal pairing occurs when the  $X^2 - Y^2$  hole Fermi surface disappears by lowering the pnictogen height. As for other origins for the presence of line nodes in the gap, the Coulomb avoidance<sup>28</sup> as well as the competition of spin and orbital fluctuations<sup>29,30</sup> has been considered.

In the present study, we consider another possibility for the origin of the gap nodes, which is peculiar to 122 materials. We construct a three dimensional ten orbital model for  $\text{BaFe}_2(\text{As}_{1-x}\text{P}_x)_2$  from first principles calculation using maximally localized Wannier orbitals,<sup>31</sup> and apply random phase approximation (RPA) to obtain the spin susceptibility and the superconducting gap function. For the 122 materials, the Brillouin zone unfolding procedure<sup>9</sup> that adopts the reduced unit cell (with one iron) cannot be done strictly,<sup>32</sup> so by adopting the ten orbital model that adopts the original unit cell (with two irons) of the body centered tetragonal lattice structure, we fully take into account the peculiar features of the 122 band structure not present in the 1111 materials. The superconducting gap is basically  $s_{\pm}$ , where the gap changes its sign between electron and hole Fermi surfaces, but when the hole Fermi surface around the Z point having strong  $3Z^2 - R^2$  ( $Z^2$ ) orbital character becomes large by isovalent doping, the superconducting gap on that Fermi surface exhibits three dimensional nodal structures. This kind of nodes is peculiar to 122 systems, as also found in a five orbital study for  $\text{BaFe}_2\text{As}_2$  (but with different orbital character of the Fermi surface).<sup>33,34</sup> Since the  $Z^2$  orbital does not play an important role in the occurrence of spin fluctuation mediated superconductivity, this explains why  $T_c$  in the isovalent doping system is relatively high despite the presence of nodes in the superconducting gap.

In order to construct a realistic model, we first perform first principles band calculation using the Quantum Espresso package<sup>35</sup> adopting the experimentally

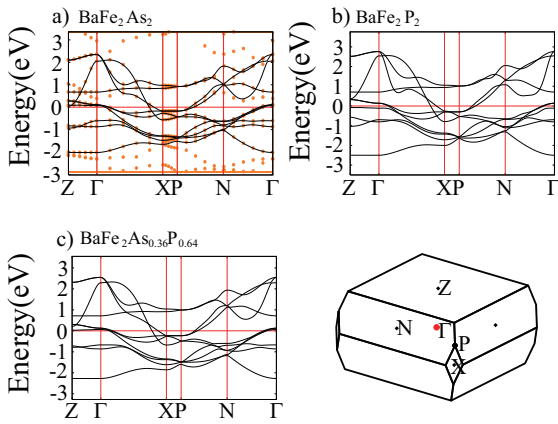


Fig. 1. Band structure of the 10 orbital model for (a)  $\text{Ba}_2\text{Fe}_2\text{As}_2$ , (b)  $\text{Ba}_2\text{Fe}_2\text{P}_2$ , and (c)  $\text{Ba}_2\text{Fe}_2\text{As}_{0.36}\text{P}_{0.64}$ . In (a), the original first principles band calculation is shown by the dots. The Brillouin zone is shown in the inset.

determined lattice structure,<sup>36</sup> and then obtain a ten orbital model using maximally localized Wannier orbitals.<sup>31</sup> There are ten bands mainly originating from the five 3d orbitals because there are two iron atoms per unit cell in the body centered tetragonal lattice structure. We show in the upper panels of Fig.1 the band structure of the ten orbital model of  $\text{Ba}_2\text{Fe}_2\text{As}_2$  and  $\text{Ba}_2\text{Fe}_2\text{P}_2$ . To obtain a model for  $\text{Ba}_2\text{Fe}_2(\text{As}_{1-x}\text{P}_x)_2$ , we first obtain a ten orbital tightbinding model for “hypothetical”  $\text{Ba}_2\text{Fe}_2\text{As}_2$  and  $\text{Ba}_2\text{Fe}_2\text{P}_2$  having the experimentally determined lattice structure of  $\text{Ba}_2\text{Fe}_2(\text{As}_{1-x}\text{P}_x)_2$  at each  $x$ . We assume that making a linear combination of the two sets of tightbinding parameters (hopping integrals and on-site energies), mixing them with the ratio of  $1-x:x$ , will give a good approximation for the band structure of  $\text{Ba}_2\text{Fe}_2(\text{As}_{1-x}\text{P}_x)_2$ . The band structure of this model with  $x = 0.64$  is shown in the lower panel of Fig.1.

In Fig.2, we show the Fermi surfaces of  $\text{Ba}_2\text{Fe}_2(\text{As}_{0.36}\text{P}_{0.64})_2$  for each orbital character, where the thickness represents the strength of the character. The 122 materials share common features with the 1111 materials in that they have three hole (around  $\Gamma$ -Z) and two electron Fermi (around X-P) surfaces. There are, however, some differences. One is that the portion of the Fermi surface around the Z point having strong  $Z^2$  character is continuously connected to the  $XZ/YZ$  portion of the Fermi surface around the  $\Gamma$  point, while in 1111 the  $Z^2$  Fermi surface, when present, is an isolated three dimensional pocket. We will call this hole Fermi surface with mixed  $Z^2$  and  $XZ/YZ$  orbital character  $\alpha_1$ . Another difference from the 1111 is that the hole Fermi surface having strong  $X^2 - Y^2$  orbital character coexists with the  $Z^2$  Fermi surface, while in 1111 either the three dimensional  $Z^2$  or the cylindrical  $X^2 - Y^2$  ( $\gamma$ ) Fermi surfaces exist depending on the pnictogen height.<sup>8,37-39</sup> The hole Fermi surface with  $X^2 - Y^2$  character will be called  $\gamma$  as in our study for 1111.<sup>8</sup> There is another hole Fermi surface having  $XZ/YZ$  character, which we will call  $\alpha_2$ .

Replacing As by P does not alter the band filling (iso-

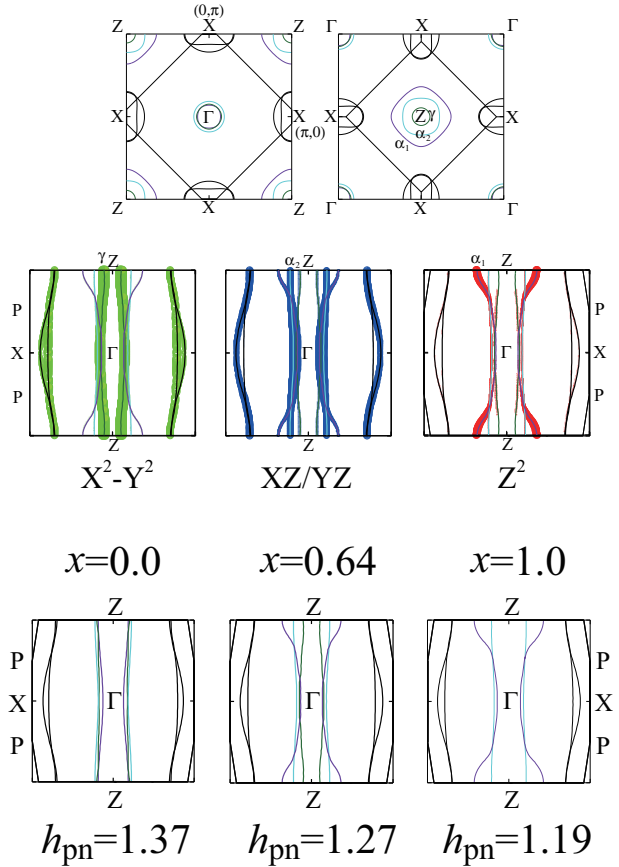


Fig. 2. Upper panels : Fermi surfaces of the ten orbital model of  $\text{Ba}_2\text{Fe}_2(\text{As}_{0.36}\text{P}_{0.64})_2$ . Horizontal (vertical) cuts are shown in the top (middle) panels. The vertical cuts are presented along with the strength of the orbital character. The X point corresponds to the wavevector  $(\pi, 0)$  in the unfolded Brillouin zone. Bottom panels : evolution of the Fermi surface upon increasing the phosphorous concentration  $x$ . The pnictogen height  $h_{\text{Pn}}$  is also presented.

valent doping), and the main effect is to reduce the pnictogen height measured from the iron planes. In the bottom panels of Fig.2, we show the vertical cut of the Fermi surface for various P content. As in 1111, lowering the height leads to a higher  $Z^2$  orbital level, resulting in a larger  $\alpha_1$  Fermi surface around the Z point.<sup>18</sup> Such a strong warping of the Fermi surface has been directly observed in a recent ARPES experiment.<sup>40</sup> At the same time, the  $X^2 - Y^2$  level is lowered, so that the  $\gamma$  Fermi surface shrinks, but it exists up to the P content of about  $x \sim 0.7$  in the present calculation.

We now move on to the RPA calculation. We mainly concentrate on  $\text{Ba}_2\text{Fe}_2(\text{As}_{0.36}\text{P}_{0.64})_2$  here, while we also comment on the calculation results for other  $x$ . As for the electron-electron interaction, we consider the intra-orbital  $U$ , the interorbital  $U'$ , the Hund’s coupling  $J$ , and the pair hopping interaction  $J'$ . We consider orbital dependent interactions obtained in ref.<sup>41</sup> We apply RPA to this model,<sup>8,9</sup> and obtain the spin and charge susceptibility matrices. From these, we obtain the pairing interaction, which are plugged into the linearized Eliashberg equation. In the RPA calculation (where the self energy correction is neglected), realistic values of the interaction

results in too large spin fluctuations, so we multiply all the electron-electron interaction by a factor  $f$ .<sup>8</sup> In this way, we keep the relative strength of the interactions between different orbitals to be the same as those obtained from first principles. In the following, we will present the eigenfunction of the Eliashberg equation in the band representation, and call them the “(superconducting) gap”. In the actual calculation results shown below, we take  $16 \times 16 \times 16$   $k$ -point meshes, 128 Matsubara frequencies,  $T = 0.07\text{eV}$ , and the interaction reducing ratio  $f = 0.55$ .

In Fig.3, we show a plot of the eigenvalue of the spin susceptibility matrix. It has a peak at the X point (corresponding to the wave vector  $(\pi, 0)$  in the unfolded Brillouin zone, although the unfolding cannot be strictly done), which originates from the interaction between electron and hole Fermi surfaces. As shown in our earlier study,<sup>8</sup> the main interaction that induces the spin fluctuation comes from the  $X^2 - Y^2$  and  $XZ/YZ$  portions of the Fermi surface, namely, the intraorbital interaction within these orbitals. Performing similar calculation for other values of  $x$ , we find that the spin susceptibility is suppressed monotonically upon increasing the phosphorous content, as expected from the fact that the  $\gamma$  Fermi surface shrinks.<sup>8</sup>

We show the superconducting gap in Fig.4. The electron and hole Fermi surfaces have different signs of the gap for most portions, namely, the gap is basically  $s\pm$ , originating from the spin fluctuation mentioned above. The gap on the electron Fermi surfaces is fully open since the  $X^2 - Y^2$   $\gamma$  Fermi surface is present, as is the case for 1111 systems with high pnictogen positions.<sup>8</sup> On the other hand, as the volume of the  $\alpha_1$  Fermi surface around the Z point grows upon lowering the pnictogen height by isovalent doping, a three dimensional sign change of the gap takes place within this Fermi surface as shown in Fig.4. The gap function on the  $\alpha_1$  Fermi surface is schematically shown in the bottom of Fig.4. This sign change can be considered as due to the repulsive intraband interaction within the  $\alpha_1$  Fermi surface (shown by the arrow in the schematic figure), which becomes more effective as the volume of the Fermi surface around the Z point grows. In fact, we find that the plus sign region of the gap on the  $\alpha_1$  Fermi surface tends to shrink for smaller values of  $x$ . A similar three dimensional sign change of the superconducting gap has been found in a five orbital study for Ba122 in ref.,<sup>33</sup> although in the model of ref.<sup>33</sup> the  $\alpha_1$  Fermi surface around the Z point has  $X^2 - Y^2$  character (or  $xy$  in the notation of ref.<sup>33</sup>) rather than  $Z^2$ .

Since the three dimensional nodes in the present study occurs at portions of the Fermi surface having strong  $Z^2$  character, the presence of the nodes does not strongly reduce  $T_c$ . This is in contrast to the case of LaFePO, where nodes of the gap, according to a similar RPA and other theoretical studies, enters in the  $X^2 - Y^2$  and/or  $XZ/YZ$  Fermi surfaces,<sup>8, 14-16, 42</sup> which play an important role in the occurrence of the spin fluctuation mediated superconductivity. The present view explains why  $T_c$  is relatively high in  $\text{BaFe}_2(\text{As}_{1-x}\text{P}_x)_2$  despite the presence of nodes in the superconducting gap.

To summarize, we have obtained a three dimensional

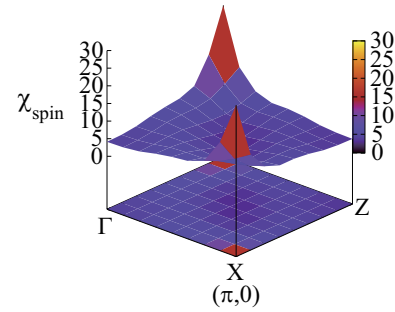


Fig. 3. The largest eigenvalue of the spin susceptibility matrix for the ten orbital model of  $\text{BaFe}_2(\text{As}_{0.36}\text{P}_{0.64})_2$ . The X point corresponds to the  $(\pi, 0)$  point in the unfolded Brillouin zone.

ten orbital model for the isovalent doping material  $\text{BaFe}_2(\text{As}_{1-x}\text{P}_x)_2$ , and applied RPA to obtain the superconducting gap originating from spin fluctuation mediated pairing. The obtained gap is basically  $s\pm$ , and we find no gap nodes on the electron Fermi surface because the  $X^2 - Y^2$   $\gamma$  Fermi surface persists up to a large P content. On the other hand, there are three dimensional nodes on the  $Z^2/XZ/YZ$  portion of the hole Fermi surface. We believe that these three dimensional nodes in the  $Z^2/XZ/YZ$  hole Fermi surface are responsible for the experimentally observed nodal behavior of the superconducting gap of  $\text{BaFe}_2(\text{As}_{1-x}\text{P}_x)_2$ , since the presence of nodes in this material does not seem to affect  $T_c$  strongly. Relation between the present view and other experimental results will be of great interest. Comparison between neutron scattering experiment and a theoretical analysis based on the present gap structure is now in progress.<sup>43</sup> It is also necessary to understand how such a gap structure on the hole Fermi surface can be consistent with the ARPES experiment,<sup>21</sup> or the apparently “nodeless” behavior observed in a specific heat experiment.<sup>44</sup> We note here that our study does not completely rule out the possibility of nodes on the electron Fermi surface, since correlation effects that are not taken into account in the present “band calculation+RPA” study may give rise to gap nodes on the electron Fermi surface (even when the  $X^2 - Y^2$  hole Fermi surface is present).<sup>14</sup> Also, there is a possibility that in the *electron* doped 122 materials, where the  $\gamma$  Fermi surface is less effective, the nodes may be on the electron Fermi surface, as suggested by a recent study.<sup>32</sup> In any case, the tendency of three dimensional nodes entering the  $Z^2/XZ/YZ$  hole Fermi surface of 122 materials should remain as far as this Fermi surface is sufficiently large and the repulsive intraband interaction is effective. In this context, a “heavily hole doped” material  $\text{KFe}_2\text{As}_2$ , mentioned as another nodal superconductor in the introductory part, is also of great interest. In fact, in our preliminary study for this material, we find a similar tendency of three dimensional gap nodes entering the  $Z^2/XZ/YZ$  hole Fermi surface. In this study, we use a model which quantitatively reproduces the spin fluctuation modes observed by a recent neutron scattering experiment.<sup>45</sup> The details will be published elsewhere.

We are grateful to Y. Matsuda, T. Shibauchi, S. Kasahara, H. Ikeda, T. Shimojima, S. Shin, Y. Nagai, S.

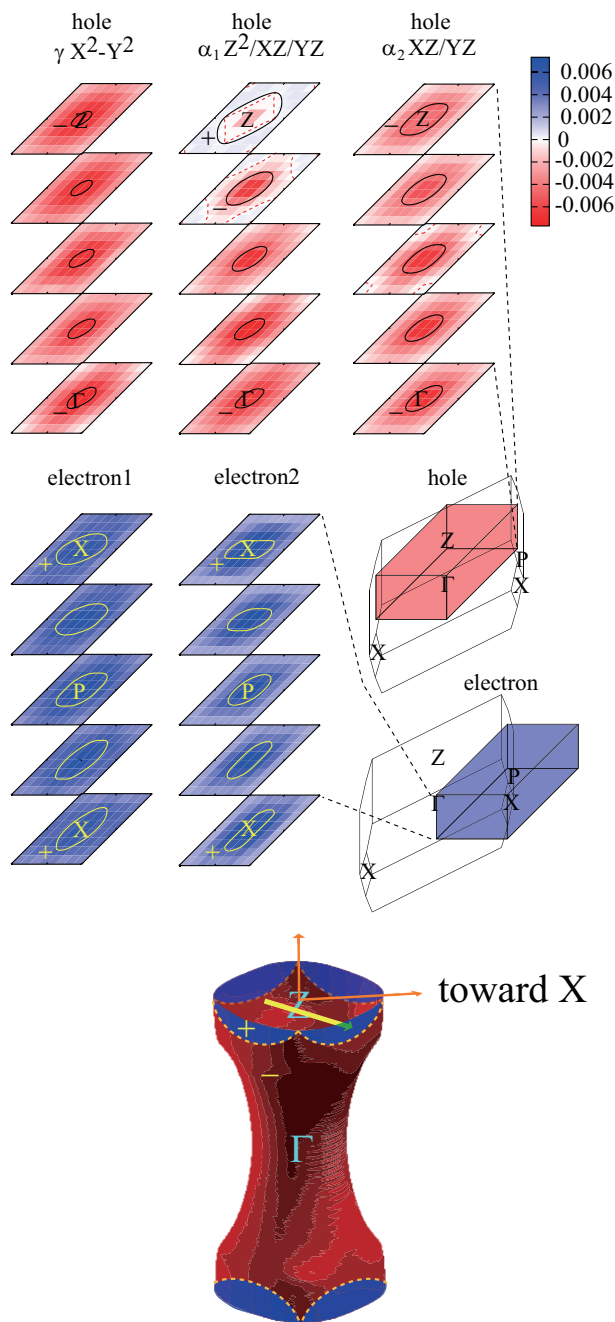


Fig. 4. The contour plots of the gap function on the five Fermi surfaces for five horizontal cuts around  $\Gamma$ -Z (hole) or X-P-X (electron). The solid lines represent the Fermi surfaces, while the dashed lines are the nodes of the gap. The Brillouin zone is shown along with the regions where the contour plots of the gap are presented. In the bottom, a schematic view of the gap function on the  $\alpha_1=Z^2/XZ/YZ$  hole Fermi surface is shown. The arrow bridging the Fermi surface indicates the intraband interaction that induces the sign change of the gap.

Shamoto, T. Yoshida, A. Fujimori, C.-H. Lee, S. Onari, R. Arita, and H. Aoki for valuable discussions. Numerical calculations were performed at the facilities of the Information Technology Center, University of Tokyo, and also at the Supercomputer Center, ISSP, University of Tokyo.

This study has been partially supported by Grant-in-Aid for Scientific Research from MEXT of Japan and from the Japan Society for the Promotion of Science.

- 1) For a review, see, e.g. K. Ishida, Y. Nakai and H. Hosono : J. Phys. Soc. Jpn. **78** (2009) 062001.
- 2) K. Hashimoto *et al.* : Phys. Rev. Lett. **102** (2009) 017002.
- 3) H. Ding *et al.* : Europhys. Lett. **83** (2008) 47001.
- 4) J.D. Fletcher *et al.* : Phys. Rev. Lett. **102** (2009) 147001.
- 5) C.W.Hicks *et al.* : arXiv: 0903.5260.
- 6) M. Yamashita *et al.* : Phys. Rev. B **80** (2009) 220509(R).
- 7) C.-H. Lee *et al.* : J. Phys. Soc. Jpn. **77** (2008) 083704.
- 8) K. Kuroki *et al.* : Phys. Rev. B **79** (2009) 224511.
- 9) K. Kuroki *et al.* : Phys. Rev. Lett. **101** (2008) 087004
- 10) I.I. Mazin *et al.* : Phys. Rev. Lett. **101** (2008) 057003.
- 11) H. Ikeda : J. Phys. Soc. Jpn. **77** (2008) 123707.
- 12) T. Nomura : J. Phys. Soc. Jpn. **78** (2009) 034716.
- 13) S.Graser *et al.* : New J. Phys. **11**, 025016 (2009).
- 14) H. Ikeda, R. Arita and J. Kunes : Phys. Rev. B **81** (2010) 054502, also private communications on further studies.
- 15) F. Wang, H. Zhai, and D.-H. Lee: Phys. Rev. B **81** (2010) 184512.
- 16) R. Thomale *et al.* : arXiv: 1002.3599.
- 17) Z. Ren *et al.* : Phys. Rev. Lett. **102** (2009) 137002.
- 18) S. Kasahara *et al.* : Phys. Rev. B **81** (2010) 184519.
- 19) K. Hashimoto *et al.* : Phys. Rev. B **81** (2010) 220501(R).
- 20) Y. Nakai *et al.* : Phys. Rev. Lett. **105** (2010) 087001.
- 21) T. Shimojima, private communication.
- 22) H. Fukazawa *et al.* : J. Phys. Soc. Jpn. **78** (2009) 083712.
- 23) J. K. Dong *et al.* : Phys. Rev. Lett. **104** (2010) 087005.
- 24) H. Kawano-Furukawa *et al.* : arXiv: 1005.4468.
- 25) S.W. Zhang *et al.* : Phys. Rev. B **81** (2010) 012503.
- 26) K. Hashimoto *et al.* : Phys. Rev. B **82**, 014526 (2010)
- 27) T. Sato *et al.* : Phys. Rev. Lett. **103** (2009) 047002.
- 28) A.V. Chubukov, M.G. Vavilov, and A.V. Vorontsov: Phys. Rev. B **80** (2009) 140515(R).
- 29) H. Kontani and S. Onari, Phys. Rev. Lett. **104** (2010) 157001.
- 30) Y. Yanagi *et al.* : Phys. Rev. B **82** (2010) 064518.
- 31) N. Marzari and D. Vanderbilt, Phys. Rev. B **56**, 12847 (1997); I. Souza, N. Marzari and D. Vanderbilt, Phys. Rev. B **65**, 035109 (2002). The Wannier functions are generated by the code developed by A. A. Mostofi, J. R. Yates, N. Marzari, I. Souza and D. Vanderbilt, (<http://www.wannier.org/>) for the energy window  $-2.4 \text{ eV} < \epsilon_k - E_F < 3.2 \text{ eV}$ , where  $\epsilon_k$  is the eigenenergy of the Bloch states and  $E_F$  the Fermi energy.
- 32) I. I. Mazin *et al.* : arXiv: 1008.0032.
- 33) S. Graser, A. F. Kemper, T. A. Maier, H.-P. Cheng, P. J. Hirschfeld, and D. J. Scalapino : Phys. Rev. B **81** (2010) 214503.
- 34) P.J. Hirschfeld and D.J. Scalapino : Physics **3** 64 (2010).
- 35) S. Baroni *et al.* : <http://www.pwscf.org/>. Here we adopt the exchange correlation functional introduced by J. P. Perdew, K. Burke, and Y. Wang (Phys. Rev. B **54**, 16533 (1996)), and the wave functions are expanded by plane waves up to a cutoff energy of 40 Ry.  $8^3$   $k$ -point meshes are used.
- 36) S. Kasahara, private communication.
- 37) D.J. Singh and M.-H. Du: Phys. Rev. Lett. **100** (2008) 237003.
- 38) S. Lebegue, Z.P. Yin, and W.E. Pickett: New J. Phys. **11**, 025004 (2009).
- 39) V. Vildosola *et al.* : Phys. Rev. B **78**, 064518 (2008).
- 40) T. Yoshida *et al.* : arXiv: 1008.2080.
- 41) T. Miyake *et al.* : J. Phys. Soc. Jpn. **79**, 044705 (2010)
- 42) T. Kariyado and M. Ogata : J. Phys. Soc. Jpn. **78** (2009) 043708.
- 43) M. Ishikado *et al.* : private communication.
- 44) J. S. Kim *et al.* : Phys. Rev. B **81** (2010) 214507.
- 45) C. -H. Lee *et al.*, arXiv: 1009.4001.